SOILS AND FOUNDATIONS Vol. 46, No. 4, 449-463, Aug. 2006
Japanese Geotechnical Society

EXTENDED TANGENTIAL-SUBLOADING SURFACE MODEL FOR GENERAL LOADING BEHAVIOR OF SOILS: APPLICATION TO NONPROPORTIONAL LOADINGS

HIDEKI SETOUCHI[i], KOICHI HASHIGUCHI[ii], TAKESHI SHIKANAI[iii] and TAKASHI OKAYASU[iv]

ABSTRACT

The conventional elastoplastic model premising that the interior of yield surface is a purely elastic domain is incapable of describing the plastic deformation by the rate of stress inside the yield surface. Thus, it is inapplicable to the description of cyclic loading behavior. Besides, the traditional elastoplastic model is independent of the stress rate component tangential to the yield surface. Therefore, it predicts an unrealistically high stiffness modulus for nonproportional loading process deviating significantly from proportional one. The *extended tangential-subloading surface model* proposed by Hashiguchi and Tsutsumi (2001) would be capable of describing the cyclic loading behavior and the inelastic strain rate induced by the stress rate component tangential to the subloading surface. In this article, the extended tangential-subloading surface model is applied to the prediction of deformation behavior of sands subjected to various loading ranging from proportional to cyclic nonproportional loading. The validity is verified by comparing with the various test data. Then, it is revealed that the incorporation of the strain rate due to the stress rate component tangential to the subloading surface is of importance for the description of nonproportional loading behavior.

Key words: elastoplasticity, nonproportional loading, subloading surface model, tangential stress rate, yield surface (**IGC**: E13)

INTRODUCTION

Elastoplastic constitutive equation for the description of general loading behavior including cyclic and nonproportional loading processes for soils has to possess the following mechanical properties.

1) The plastic deformation is induced by the rate of stress inside the yield surface. Thus, the constitutive equation has to fall within the framework of the *unconventional plasticity* (Drucker, 1988). This property is inevitably necessary for the description of cyclic loading behavior, and is also required for the description of softening behavior. Its description has been attained by the subloading surface model (Hashiguchi and Ueno, 1977; Hashiguchi, 1978, 1989).
2) The *Masing effect* (Masing, 1926), i.e. the decrease in the curvature of the stress-strain curve in the reverse loading from that in the initial loading has to be incorporated, while the properties 1) and 2) could be described by the *extended subloading surface model* (Hashiguchi, 1989). Here, notes that the other unconventional models, e.g. the *multi surface model* (Mroz, 1967; Iwan, 1967), the *two surface model* (Dafalias, 1975; Krieg, 1975) and the *nonlinear-kinematic hardening model* (Armstrong and Fredericson, 1966; Lemaitre and Chaboche, 1990) cannot describe the *Masing effect* (Masing, 1926) appropriately have been reviewed by Hashiguchi (1993a, b, 1997).
3) The plastic strain rate is induced only by the stress rate component normal to the yield surface, called the *normal stress rate*, in the traditional elastoplasticity. The significant inelastic strain rate is induced by the stress rate component tangential to the yield surface, called the *tangential stress rate*, in the nonproportional loading process observed in the plastic instability phenomena. Here, it is called the *tangential stress rate effect*. It can be described appropriately by the *extended tangential-subloading surface model* (Hashiguchi, 1998; Hashiguchi and Tsutsumi, 2001).

[i] Research Associate, Department of Environmental Sciences and Technology, University of the Ryukyus, Japan (setouchi@agr.u-ryukyu.ac.jp).
[ii] Professor, Graduate School of Kyushu University, Division of Bioproduction Environmental Science, Japan.
[iii] Associate Professor, Department of Bioproduction, University of the Ryukyus, Japan.
[iv] Associate Professor, Graduate School of Kyushu University, Division of Bioproduction Environmental Science, Japan.
The manuscript for this paper was received for review on June 29, 2005; approved on March 10, 2006.
Written discussions on this paper should be submitted before March 1, 2007 to the Japanese Geotechnical Society, 4-38-2, Sengoku, Bunkyo-ku, Tokyo 112-0011, Japan. Upon request the closing date may be extended one month.

4) The *continuity* and the *smoothness conditions* (Hashiguchi, 1993a, b, 1997, 2000) have to be fulfilled, while the unconventional models other than the subloading surface model, e.g. the multi surface model (Mroz, 1967; Iwan, 1967), the two surface model (Dafalias, 1975; Krieg, 1975) and the nonlinear-kinematic hardening model (Armstrong and Fredericson, 1966; Lemaitre and Chaboche, 1990) do not fulfill the smoothness condition. Thus they violate also the continuity condition if the inelastic strain rate due to the tangential stress rate as has been suggested by Hashiguchi (2005), while the properties 1)-4) could be attained by the *extended tangential-subloading surface model* (Hashiguchi, 1998; Hashiguchi and Tsutsumi, 2001). The following isotropic and anisotropic hardenings have to be incorporated for soils.
5) The isotropic hardening of soils is substantially given by the plastic volumetric strain. Further, the equivalent strain (the accumulation of the magnitude of deviatoric strain increment), called the *deviatoric hardening* (Nova, 1977; Wilde, 1977; Hashiguchi and Chen, 1998), has to be incorporated for the isotropic hardening of sands.
6) The *rotational hardening* (Sekiguchi and Ohta, 1977; Hashiguchi and Chen, 1998; Hashiguchi, 2001), i.e. the rotation of yield surface is incorporated in order to describe the inherent/induced anisotropy.

In this article, the extended tangential-subloading surface model with the rotational and volumetric-deviatoric hardenings is applied for the prediction of deformation behavior of sands. Then, it is verified by comparisons with test data that the model has the high capability of describing the deformation behavior for a wide range from the proportional to the cyclic-nonproportional loading processes. In particular it is revealed that the tangential stress rate effect is of importance for the description of nonproportional loading behavior.

The signs of stress (rate) and strain rate components are taken to be positive for tension throughout this article.

OUTLINE OF THE EXTENDED TANGENTIAL-SUBLOADING SURFACE MODEL

In this section the tangential-subloading surface model based on the extended subloading surface model (Hashiguchi and Tsutsumi, 2001) is reviewed briefly, which will be later applied to the analyses of the deformation behavior in sands subjected to the nonproportional loading.

Denoting the current configuration of material particle as $\mathbf{x}$ and the current velocity as $\mathbf{v}$, the velocity gradient is described by $\mathbf{L}\equiv\partial\mathbf{v}/\partial\mathbf{x}$, by which the strain rate and the continuum spin are defined as $\mathbf{D}(\equiv(\mathbf{L}+\mathbf{L}^{\mathrm{T}})/2)$ and $\mathbf{W}(\equiv(\mathbf{L}-\mathbf{L}^{\mathrm{T}})/2)$, respectively, $(\ )^{\mathrm{T}}$ standing for the transpose.

Now assuming that the strain rate $\mathbf{D}$ is additively decomposed into the elastic strain rate $\mathbf{D}^{\mathrm{e}}$ and the inelastic strain rate $\mathbf{D}^{\mathrm{i}}$ which is further decomposed into the plastic strain rate $\mathbf{D}^{\mathrm{p}}$ and the *tangential strain rate* $\mathbf{D}^{\mathrm{t}}$, we have;

$$\mathbf{D}=\mathbf{D}^{\mathrm{e}}+\mathbf{D}^{\mathrm{i}}, \tag{1}$$

$$\mathbf{D}^{\mathrm{i}}=\mathbf{D}^{\mathrm{p}}+\mathbf{D}^{\mathrm{t}}, \tag{2}$$

where the elastic strain rate $\mathbf{D}^{e}$ is given by;

$$\mathbf{D}^{\mathrm{e}}=\mathbf{E}^{-1}\mathring{\boldsymbol{\sigma}}. \tag{3}$$

$\boldsymbol{\sigma}$ is the *Cauchy stress* and $(^{\circ})$ indicates the proper corotational rate with the objectivity (e.g. Dafalias, 1985; Zbib and Aifantis, 1988) and the fourth-order tensor $\mathbf{E}$ is the elastic modulus given in the Hooke's type as;

$$E_{ijkl}=\left(K-\frac{2}{3}G\right)\delta_{ij}\delta_{kl}+G(\delta_{ik}\delta_{jl}+\delta_{il}\delta_{jk}), \tag{4}$$

where K and G are the bulk and shear modulus, respectively, which are functions of stress and internal state variables in general and δ_{ij} is the Kronecker's delta, i.e. $\delta_{ij}=1$ for $i=j$ and $\delta_{ij}=0$ for $i\neq j$.

Normal-Yield and Subloading Surfaces

Assume the yield condition:

$$f(\hat{\boldsymbol{\sigma}},\mathbf{H})=F(H), \tag{5}$$

where

$$\hat{\boldsymbol{\sigma}}\equiv\boldsymbol{\sigma}-\boldsymbol{\alpha}. \tag{6}$$

The second-order tensor $\boldsymbol{\alpha}$ is the reference point inside the yield surface, which plays the role of the kinematic hardening variable as it translates with the plastic deformation. The second-order tensor $\mathbf{H}$ and the scalar H are the inherent or induced anisotropic hardening and isotropic hardening/softening variables, respectively. Let it be assumed that the function f is homogeneous of degree one in the tensor $\hat{\boldsymbol{\sigma}}$, satisfying $f(s\hat{\boldsymbol{\sigma}},\mathbf{H})=sf(\hat{\boldsymbol{\sigma}},\mathbf{H})$ for any nonnegative scalar s. Then, if $\mathbf{H}=$const., the yield surface keeps the similar shape and translates with $\boldsymbol{\alpha}$. The inherent and the induced anisotropy of soils can be described concisely by the *rotational hardening*, whilst the kinematic hardening is inapplicable to soils as has been described by Hashiguchi (2001).

Hereinafter, let the elastoplastic constitutive equation be formulated in the framework of the *unconventional plasticity* defined by Drucker (1988) as the extended plasticity such that the interior of yield surface is not a purely elastic domain but plastic deformation is induced by the rate of stress inside the yield surface. Thus, the conventional yield surface is renamed as the *normal-yield surface*, since its interior is not regarded to be a purely elastic domain in the present model.

Now, let the *subloading surface* (Hashiguchi and Ueno, 1977; Hashiguchi, 1980, 1989) be introduced, which always passes through the current stress $\boldsymbol{\sigma}$ and keeps the similarity and the configuration of similarity to the normal-yield surface. All lines passing through arbitrary conjugate pair of points on these surfaces joint at the specified point, i.e. the *similarity-center* which will be denoted by $\mathbf{s}$. In addition, assuming the subloading

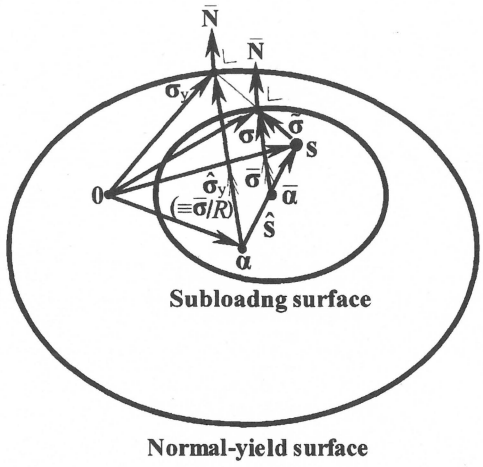

Fig. 1. Normal-yield and subloading surfaces

surface, which plays the role of loading surface, does not intersect the normal-yield surface, we have that the similarity-center has to lie inside the normal-yield surface. The ratio of the size of the subloading surface to that of the normal-yield surface will be denoted by $R(0 \leq R \leq 1)$ which can be regarded as the measure of approaching degree to the normal-yield state and is thus called the *normal-yield ratio*. The conjugate stress σ_y on the normal-yield surface for the current stress σ on the subloading surface due to the similarity is given by;

$$\sigma_y = \frac{1}{R}\{\sigma - (1-R)s\} \quad (\sigma - s = R(\sigma_y - s)). \tag{7}$$

By substituting Eq. (7) into Eq. (5) with regarding $\hat{\sigma}$ in Eq. (5) as σ_y, the subloading surface is described as;

$$f(\bar{\sigma}, H) = RF(H), \tag{8}$$

where

$$\bar{\sigma} \equiv \sigma - \bar{\alpha}, \tag{9}$$

$$\bar{\alpha} \equiv s - R(s - \alpha). \tag{10}$$

Here $\bar{\alpha}$ inside the subloading surface is the conjugate point of α inside the normal-yield surface. The normal-yield and the subloading surfaces are illustrated in Fig. 1.

Evolution of Normal-Yield Ratio

Taking account of the fact that a stress asymptotically approaches the normal-yield surface, i.e. that the subloading surface approaches the normal-yield surface in the plastic loading process, let the evolution rule of the normal-yield ratio R be given by;

$$\dot{R} = U\|\mathbf{D}^p\| \text{ for } \mathbf{D}^p \neq \mathbf{0}, \tag{11}$$

where U is the monotonically decreasing function of R, satisfying

$$\left.\begin{array}{ll} U = +\infty & \text{for } R = 0, \\ U = 0 & \text{for } R = 1, \\ (U < 0 & \text{for } R > 1). \end{array}\right\} \tag{12}$$

$(\dot{\ })$ stands for the material-time derivative, $\| \ \|$ stands for the magnitude, i.e. $\|\mathbf{T}\| = \sqrt{\mathrm{tr}(\mathbf{T}\mathbf{T}^T)}$, tr( ) denoting the trace. Let the function U satisfying Eq. (12) be simply given by;

$$U = -u_R \ln R, \tag{13}$$

where u_R is a material constant.

Translation Rule of Similarity-Center

The similarity-center s is required to translate with the plastic deformation in order to describe realistically the cyclic loading behavior exhibiting the Masing effect (Mashing, 1926; Mroz, 1966; Hashiguchi, 1993b). The translation rule of the similarity-center s is given as

$$\mathring{\mathbf{s}} = c_s\|\mathbf{D}^p\|\frac{\tilde{\sigma}}{R} + \mathring{\alpha} + \frac{1}{F}\left\{\dot{F} - \mathrm{tr}\left(\frac{\partial f(\hat{\mathbf{s}}, \mathbf{H})}{\partial \mathbf{H}}\mathring{\mathbf{H}}\right)\right\}\hat{\mathbf{s}}, \tag{14}$$

where

$$\tilde{\sigma} \equiv \sigma - \mathbf{s}, \tag{15}$$

$$\hat{\mathbf{s}} \equiv \mathbf{s} - \alpha. \tag{16}$$

c_s is a material constant.

Plastic Strain Rate

The time-differentiation of Eq. (8) yields the *extended consistency condition* for the subloading surface:

$$\mathrm{tr}\left(\frac{\partial f(\bar{\sigma}, \mathbf{H})}{\partial \sigma}\mathring{\sigma}\right) - \mathrm{tr}\left(\frac{\partial f(\bar{\sigma}, \mathbf{H})}{\partial \sigma}\mathring{\bar{\alpha}}\right) + \mathrm{tr}\left(\frac{\partial f(\bar{\sigma}, \mathbf{H})}{\partial \mathbf{H}}\mathring{\mathbf{H}}\right) = U\|\mathbf{D}^p\|F + RF'\dot{H}, \tag{17}$$

where

$$F' \equiv \frac{dF}{dH}. \tag{18}$$

Assuming the *associated flow rule* for the subloading surface, we have

$$\mathbf{D}^p = \lambda\bar{\mathbf{N}}, \tag{19}$$

$$\bar{\mathbf{N}} \equiv \frac{\partial f(\bar{\sigma}, \mathbf{H})}{\partial \sigma}\Big/\left\|\frac{\partial f(\bar{\sigma}, \mathbf{H})}{\partial \sigma}\right\| \quad (\|\bar{\mathbf{N}}\| = 1), \tag{20}$$

where λ is the positive proportionality factor. The second-order tensor $\bar{\mathbf{N}}$ is the normalized outward-normal of the subloading surface.

The substitution of Eq. (19) into the extended consistency condition (17) leads to

$$\lambda = \frac{\mathrm{tr}(\bar{\mathbf{N}}\mathring{\sigma})}{\bar{M}_p}, \tag{21}$$

where

$$\bar{M}_p \equiv \mathrm{tr}\left[\bar{\mathbf{N}}\left(\left\{\frac{F'}{F}h - \frac{1}{RF}\mathrm{tr}\left(\frac{\partial f(\bar{\sigma}, \mathbf{H})}{\partial \mathbf{H}}\mathbf{h}\right) + \frac{U}{R}\right\}\bar{\sigma} + \bar{\alpha}\right)\right]. \tag{22}$$

h, $\mathbf{h}$ and $\bar{\mathbf{a}}$ are the functions of the stress, plastic internal state variables and $\bar{\mathbf{N}}$ in degree one. These functions are related to $\dot{H}$, $\mathring{\mathbf{H}}$ and $\mathring{\bar{\alpha}}$ by

$$h \equiv \frac{\dot{H}}{\lambda}, \quad \mathbf{h} \equiv \frac{\dot{\mathbf{H}}}{\lambda}, \tag{23}$$

$$\bar{\mathbf{a}} \equiv \frac{\mathring{\alpha}}{\lambda} = \mathbf{z} - U(\mathbf{s}-\boldsymbol{\alpha}) - R(\mathbf{z}-\mathbf{a}), \tag{24}$$

$$\mathbf{a} \equiv \frac{\mathring{\alpha}}{\lambda}, \tag{25}$$

$$\mathbf{z} \equiv \frac{\mathring{\mathbf{s}}}{\lambda} = c_s \frac{\tilde{\boldsymbol{\sigma}}}{R} + \mathbf{a} + \frac{1}{F}\left\{F'h - \mathrm{tr}\left(\frac{\partial f(\hat{\mathbf{s}}, \mathbf{H})}{\partial \mathbf{H}}\mathbf{h}\right)\right\}\hat{\mathbf{s}} \tag{26}$$

since $\dot{H}$, $\dot{\mathbf{H}}$ and $\mathring{\alpha}$ include λ in degree one.

Tangential Strain Rate

Let it be assumed that the tangential strain rate is induced by the stress rate component tangential to the subloading surface, called the *tangential stress rate*. Here, assume further that the tangential strain rate is induced only by the deviatoric component of tangential stress rate, obeying the Rudnicki and Rice's (1975) conclusion that "no vertex can result from hydrostatic stress increments" based on the consideration of the sliding mechanism in the fissure model.

The tangential strain rate $\mathbf{D}^t$ is formulated as

$$\mathbf{D}^t = \frac{1}{T}\mathring{\boldsymbol{\sigma}}_t^*, \tag{27}$$

where T is a monotonically decreasing function of R satisfying the following condition.

$$\left.\begin{aligned} T &= \infty \quad \text{for} \quad R = 0, \\ T &= \xi \quad \text{for} \quad R = 1, \end{aligned}\right\} \tag{28}$$

ξ being a material function of the stress and the plastic internal variables in general. The function T, called the *tangential inelastic modulus*, satisfying Eq. (28) is simply given by

$$T = \frac{\xi}{R^{b_T}}, \tag{29}$$

where $b_T (\geq 1)$ is a material constant. The second-order tensor $\mathring{\boldsymbol{\sigma}}_t^*$ is given as follows:

$$\mathring{\boldsymbol{\sigma}}_t^* \equiv \mathring{\boldsymbol{\sigma}}^* - \mathring{\boldsymbol{\sigma}}_n^*, \tag{30}$$

$$\mathring{\boldsymbol{\sigma}}_n^* \equiv \mathrm{tr}(\bar{\mathbf{n}}^* \mathring{\boldsymbol{\sigma}}^*)\bar{\mathbf{n}}^*, \tag{31}$$

$$\mathring{\boldsymbol{\sigma}}^* \equiv \mathring{\boldsymbol{\sigma}} - \dot{\sigma}_m \mathbf{I}, \quad \sigma_m \equiv \frac{1}{3}\mathrm{tr}\,\boldsymbol{\sigma}, \tag{32}$$

$$\bar{\mathbf{n}}^* \equiv \left(\frac{\partial f(\bar{\boldsymbol{\sigma}}, \mathbf{H})}{\partial \boldsymbol{\sigma}}\right)^* \Big/ \left\|\left(\frac{\partial f(\bar{\boldsymbol{\sigma}}, \mathbf{H})}{\partial \boldsymbol{\sigma}}\right)^*\right\| = \frac{\bar{\mathbf{N}}^*}{\|\bar{\mathbf{N}}^*\|} \quad (\|\bar{\mathbf{n}}^*\| = 1), \tag{33}$$

$$\bar{\mathbf{N}}^* \equiv \left(\frac{\partial f(\bar{\boldsymbol{\sigma}}, \mathbf{H})}{\partial \boldsymbol{\sigma}}\right)^* \Big/ \left\|\left(\frac{\partial f(\bar{\boldsymbol{\sigma}}, \mathbf{H})}{\partial \boldsymbol{\sigma}}\right)\right\| \quad (\|\bar{\mathbf{N}}^*\| \neq 1). \tag{34}$$

$(\ )^*$ stands for the deviatoric part and $\mathbf{I}$ is the identity tensor. $\bar{\mathbf{n}}^*$ is the normalized deviatoric outward-normal tensor of the subloading surface. The stress rate $\mathring{\boldsymbol{\sigma}}_t^*$ is called the *deviatoric tangential stress rate* fulfilling

$$\mathrm{tr}(\bar{\mathbf{N}}\mathring{\boldsymbol{\sigma}}_t^*) = 0, \quad \mathrm{tr}\,\mathring{\boldsymbol{\sigma}}_t^* = 0. \tag{35}$$

The deviatoric tangential stress rate $\mathring{\boldsymbol{\sigma}}_t^*$ is directed toward the tangential line of the closed curve formed by the intersection of the subloading surface and the deviatoric stress plane as illustrated in Fig. 2. The tangential strain rate $\mathbf{D}^t$ is related linearly to the deviatoric tangential stress rate $\mathring{\boldsymbol{\sigma}}_t^*$ through the normal-yield ratio R so as to exhibit the smooth elastic-inelastic transition. Besides, it can be formulated so as to be hardly induced when a stress lies inside the normal-yield surface by giving a large value to the material parameter b_T.

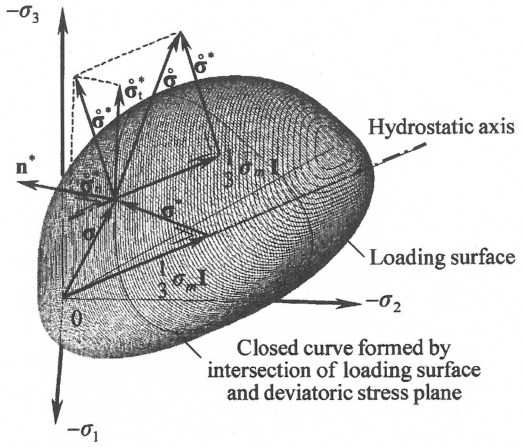

Fig. 2. The deviatoric tangential stress rate $\mathring{\boldsymbol{\sigma}}_t^*$ illustrated in principal stress space

The strain rate $\mathbf{D}$ is given from Eqs. (1), (2), (3), (19) and (27) as

$$\mathbf{D} = \mathbf{E}^{-1}\mathring{\boldsymbol{\sigma}} + \frac{\mathrm{tr}(\bar{\mathbf{N}}\mathring{\boldsymbol{\sigma}})}{\bar{M}_p}\bar{\mathbf{N}} + \frac{1}{T}\mathring{\boldsymbol{\sigma}}_t^*. \tag{36}$$

The inverse expression of Eq. (36) is given as

$$\mathring{\boldsymbol{\sigma}} = \frac{1}{1+\dfrac{2G}{T}}\left\{\mathbf{ED} - \frac{\mathrm{tr}(\bar{\mathbf{N}}\mathbf{ED})}{\bar{M}_p + \mathrm{tr}(\bar{\mathbf{N}}\mathbf{E}\bar{\mathbf{N}})}\left[\mathbf{E}\bar{\mathbf{N}} + \frac{2G}{T}\left\{\frac{1}{3}\mathrm{tr}(\mathbf{E}\bar{\mathbf{N}})\mathbf{I} - \left(\bar{M}_p + \frac{1}{3}\mathrm{tr}\bar{\mathbf{N}}\mathrm{tr}(\mathbf{E}\bar{\mathbf{N}})\right)\frac{\bar{\mathbf{n}}^*}{\|\bar{\mathbf{N}}^*\|}\right\}\right] + \frac{2G}{T}\mathrm{tr}(\mathbf{ED})\left(\frac{1}{3}\mathbf{I} - \frac{1}{3}\mathrm{tr}\bar{\mathbf{N}}\frac{\bar{\mathbf{n}}^*}{\|\bar{\mathbf{N}}^*\|}\right)\right\}. \tag{37}$$

The positive proportionality factor in the associated flow rule (19) is expressed in terms of the strain rate $\mathbf{D}$, rewriting λ as Λ, as follows:

$$\Lambda = \frac{\mathrm{tr}(\bar{\mathbf{N}}\mathbf{ED})}{\bar{M}_p + \mathrm{tr}(\bar{\mathbf{N}}\mathbf{E}\bar{\mathbf{N}})} \tag{38}$$

because of $\mathrm{tr}(\bar{\mathbf{N}}\mathbf{E}\mathring{\boldsymbol{\sigma}}_t^*) = 0$ for Eq. (4).

Loading Criterion

The loading criterion is given by the positiveness of the proportionality factor Λ as follows (Hashiguchi, 2000):

$$\left.\begin{aligned} \mathbf{D}^p \neq \mathbf{0}&: \Lambda > 0, \\ \mathbf{D}^p = \mathbf{0}&: \Lambda \leq 0. \end{aligned}\right\} \tag{39}$$

MATERIAL FUNCTIONS OF SOILS

Based on the equations formulated in the previous section and the model proposed by Hashiguchi and Chen (1998), the particular forms of the material functions for soils will be given in this section. Hereafter, our focus of attention will be on the behavior of the saturated soils, and then let the *Cauchy stress* $\boldsymbol{\sigma}$ be meant the *effective Cauchy stress* excluded a pore pressure from the *total Cauchy stress*.

Let the stress function in the subloading surface (8) be given for soils as

$$f(\bar{\boldsymbol{\sigma}}, \boldsymbol{\beta}) = \bar{p}(1+\bar{\chi}^2), \tag{40}$$

where

$$\bar{\boldsymbol{\sigma}}^* \equiv \bar{\boldsymbol{\sigma}} + \bar{p}\mathbf{I}, \quad \bar{p} \equiv -\frac{1}{3}\operatorname{tr}\bar{\boldsymbol{\sigma}}, \quad \bar{\chi} \equiv \frac{\|\bar{\boldsymbol{\eta}}\|}{\bar{m}}, \tag{41}$$

$$\bar{\boldsymbol{\eta}} \equiv \bar{\mathbf{Q}} - \boldsymbol{\beta}, \quad \bar{\mathbf{Q}} \equiv \frac{\bar{\boldsymbol{\sigma}}^*}{\bar{p}}. \tag{42}$$

The anisotropic hardening variable $\mathbf{H}$ is selected as the rotational hardening variable $\boldsymbol{\beta}$ (Sekiguchi and Ohta, 1977). $\bar{m}$ is the stress ratio in the critical state, which is generally a function f_{m} of

$$\cos 3\bar{\theta}_\sigma \equiv \sqrt{6}\operatorname{tr}\left(\frac{\bar{\boldsymbol{\eta}}}{\|\bar{\boldsymbol{\eta}}\|}\right)^3 \tag{43}$$

including the material constant ϕ_{c} referred to the frictional angle in the critical state for the axisymmetric compression, i.e.

$$\bar{m} = f_{\mathrm{m}}(\cos 3\bar{\theta}_\sigma;\ \phi_{\mathrm{c}}). \tag{44}$$

The evolution rule of rotational hardening variable $\boldsymbol{\beta}$ is given as follows (Hashiguchi and Chen, 1998; Hashiguchi, 2001):

$$\overset{\circ}{\boldsymbol{\beta}} = b_{\mathrm{r}}\|\mathbf{D}^{\mathrm{p}^*}\|\|\bar{\boldsymbol{\eta}}\|\bar{\boldsymbol{\eta}}_{\mathrm{b}}, \tag{45}$$

where

$$\bar{\boldsymbol{\eta}}_{\mathrm{b}} \equiv \bar{m}_{\mathrm{b}}\bar{\mathbf{t}} - \boldsymbol{\beta}, \quad \bar{\mathbf{t}} \equiv \frac{\bar{\boldsymbol{\eta}}}{\|\bar{\boldsymbol{\eta}}\|}. \tag{46}$$

$\bar{m}_{\mathrm{b}}$ is the function f_{m} of $\bar{\theta}_\sigma$ including the material constant ϕ_{b}, i.e.

$$\bar{m}_{\mathrm{b}} = f_{\mathrm{m}}(\cos 3\bar{\theta}_\sigma;\ \phi_{\mathrm{b}}). \tag{47}$$

b_{r} is the material constant describing the intensity of rotational hardening. ϕ_{b} is the material constant describing the limitation of the rotation of the subloading surface, called the *rotational limit angle*, and the surface described by the following equation is called the *rotational limit surface*.

$$\frac{\|\boldsymbol{\sigma}^*\|}{p} = \bar{m}_{\mathrm{b}}. \tag{48}$$

The isotropic hardening/softening function F is given by;

$$F = F_0 \exp\left(\frac{H}{\rho - \gamma}\right), \tag{49}$$

where F_0 is the initial value of F. ρ and γ are material constants describing the slope of the normal-consolidation and the swelling lines, respectively, in $(\ln v,\ \ln p)$ space (v: volume) (Hashiguchi, 1974, 1995). The evolution rule of the isotropic hardening/softening variable H applicable to not only clays but also sands is given as follows (Nova, 1977; Wilde, 1977; Hashiguchi and Chen, 1998):

$$\dot{H} = -D_{\mathrm{v}}^{\mathrm{p}} + \mu\|\mathbf{D}^{\mathrm{p}^*}\|\left(\frac{\|\boldsymbol{\sigma}^*\|}{p} - m_{\mathrm{d}}\right), \tag{50}$$

where

$$D_{\mathrm{v}}^{\mathrm{p}} \equiv \operatorname{tr}\mathbf{D}^{\mathrm{p}}, \tag{51}$$

$$p \equiv -\frac{1}{3}\operatorname{tr}\boldsymbol{\sigma}. \tag{52}$$

m_{d} is given as;

$$m_{\mathrm{d}} = f_{\mathrm{m}}(\cos 3\theta_\sigma;\ \phi_{\mathrm{d}}), \tag{53}$$

where θ_σ is the Lode angle, i.e.

$$\cos 3\theta_\sigma \equiv \sqrt{6}\operatorname{tr}\left(\frac{\boldsymbol{\sigma}^*}{\|\boldsymbol{\sigma}^*\|}\right)^3. \tag{54}$$

μ and ϕ_{d} are material constants describing the isotropic hardening/softening behavior induced by the plastic deviatoric deformation. The softening and the hardening are induced by the plastic deviatoric deformation for the state of stress inside and outside, respectively, the surface:

$$\frac{\|\boldsymbol{\sigma}^*\|}{p} = m_{\mathrm{d}}, \tag{55}$$

which is called the *shear boundary surface*.

Let the function ξ in the tangential inelastic modulus T be assumed as

$$\xi = \frac{p}{a_{\mathrm{T}}\bar{\chi}^{c_{\mathrm{T}}}}, \tag{56}$$

where a_{T} and c_{T} are material constants. It is verified by Iizuka et al. (2005) that the tangential strain rate Eq. (27) with Eqs. (29) and (56) can predict appropriately the decrease of the instantaneous shear modulus observed in the experimental data of sand, while the modulus based on the former formulation of Yatomi et al.'s (1989) exhibits the opposite trend to the experimental data.

The elastic bulk and shear moduli are given as;

$$K = \frac{p}{\gamma}, \quad G = \frac{3(1-2\nu)}{2(1+\nu)}K, \tag{57}$$

where ν is *Poisson's ratio*.

The fulfillment of the convexity in the yield surface is desirable for the formulation of variational principles as represented by the principle of maximum plastic work (cf. e.g. Hill, 1950). Besides, the convexity of the yield surface is required for the formulation of the evolution rule of the similarity-center of the normal-yield and the subloading surfaces in the extended subloading surface model (Hashiguchi, 1989). Yield surfaces of soils are usually formulated in the form involving an equation of

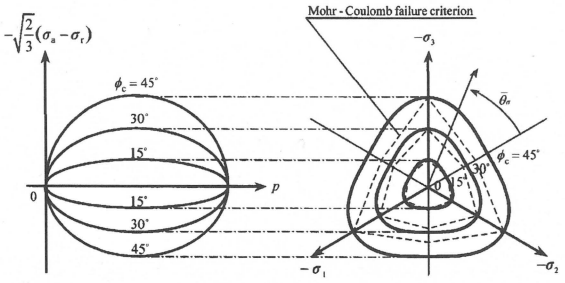

Fig. 3. Normal-yield surfaces in $(p, -\sqrt{2/3}(\sigma_a-\sigma_r))$ plane with the sections by π-plane

the *critical state surface*. Therefore, the convexity of the critical state surface is required, which exhibits a conical shape described approximately by the Mohr-Coulomb criterion in principal stress space. The following equation proposed by Hashiguchi (2002) is adopted as the function $\bar{m}$ fulfilling the above-mentioned requirements.

$$\bar{m}=\frac{14\sqrt{6}\,\sin\phi_c}{(3-\sin\phi_c)(8+\cos 3\bar{\theta}_\sigma)}. \tag{58}$$

The sections of the surface $\|\bar{\mathbf{Q}}\|=\bar{m}$ by the $(p, -\sqrt{2/3}(\sigma_a-\sigma_r))$ plane and by the π-plane for $\phi_c=15$, 30, and 45° are depicted in Fig. 3, where σ_a and σ_r are the axis and radial stresses. The surfaces are smooth and fulfill the convexity for any frictional angle ϕ_c as shown in the figure, while it gives rise to a slightly higher frictional angle in the axisymmetric extension state than that in the axisymmetric compression state for a high frictional angle (Hashiguchi, 2002). The functions $\bar{m}_b$ and m_d in Eqs. (47) and (53) for the rotational limit and shear boundary surfaces are given as follows:

$$\bar{m}_b=\frac{14\sqrt{6}\,\sin\phi_b}{(3-\sin\phi_b)(8+\cos 3\bar{\theta}_\sigma)}, \tag{59}$$

$$\bar{m}_d=\frac{14\sqrt{6}\,\sin\phi_d}{(3-\sin\phi_d)(8+\cos 3\bar{\theta}_\sigma)}. \tag{60}$$

COMPARISONS WITH EXPERIMENTS

The validity of the extended tangential-subloading surface model with the material functions for soils described in the previous sections is verified in this section by comparing with the test data of the sands, i.e. the Reid Bedford sand, the Hostun sand (Saada and Bianchini, 1989) and Toyoura sand (Tatsuoka et al., 1986; Pradhan et al., 1989). The comparison with the test data of Hostun sand has been reported already by Hashiguchi and Chen (1998) where the tangential strain rate has not been incorporated. Then, only the comparison with the test data for nonproportional loading behavior is performed, in which a significant tangential stress rate is induced.

Both the Reid Bedford sand and the Hostun sand are poorly graded materials with uniform grain size. Their physical properties are listed in Table 1. The specimens were prepared at the medium state of void ratio $e_0=0.67$ for Reid Bedford sand and at the dense state of void ratio

Table 1. Physical properties of Reid Bedford sand and Hostun sand

	Reid Bedford sand	Hostun sand
Percent of sand (%)	99.43	99.55
Grain density (g/cm^3)	2.65	2.67
Maximum density (g/cm^3)	1.74	1.66
Minimum density (g/cm^3)	1.46	1.35
Mean grain size (mm)	0.25	0.35
Uniformity coefficient	1.47	1.68

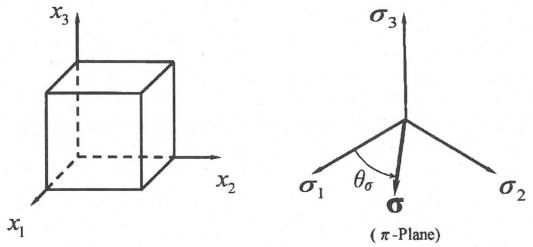

Fig. 4. Rectangular co-ordinates (x_1, x_2, x_3) and the variables for the true triaxial test apparatus

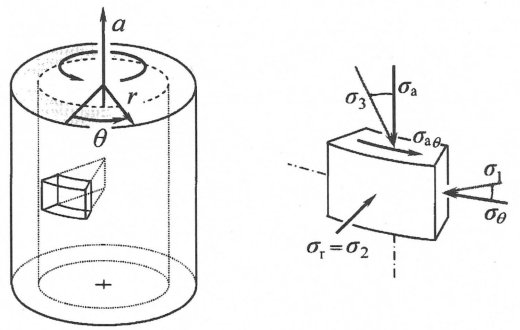

Fig. 5. Cylindrical co-ordinates (θ, r, a) for the hollow cylinder test apparatus

$e_0=0.62$ for Hostun sand under the initial isotropic states of stress $\sigma_0=-100$ kPa. The tests were performed under the drained condition by the true triaxial test apparatus and the hollow cylinder test apparatus.

The co-ordinate system (x_1, x_2, x_3) is taken for the true triaxial test apparatus as shown in Fig. 4 where σ_1, σ_2, σ_3 are the principal stresses. The co-ordinate system (θ, r, a) is taken for the hollow cylinder test apparatus as shown in Fig. 5 where σ_θ, σ_r, σ_a and $\sigma_{a\theta}$ are the peripheral stress, the radial stress, the axial stress and the torsional shear stress, respectively. Strain components ε_{ij} are calculated by the time-integration of strain rate component D_{ij}, assuming that the rotation of material is negligible.

In all analyses, the deviatoric stress is loaded after the isotropic loading from the initial isotropic stress state $\sigma_0=-100$ kPa to the prescribed isotropic stress $\sigma_{m0}=-345$ kPa for Reid Bedford sand and $\sigma_{m0}=-500$ kPa for Hostun.

Table 2. Types of test for the proportional loading

Apparatus	Type of test	b-value	Stress increment
True tiaxial (cubical)	Cyclic isotropic loading	—	$\Delta\sigma_1=\Delta\sigma_2=\Delta\sigma_3$
	Axisymmetic compression	0	$\Delta\sigma_3<0,\ \Delta\sigma_1=\Delta\sigma_2=0$
	Compression	0.277	$\Delta\sigma_1/\Delta\sigma_3=-0.383,\ \Delta\sigma_3<0,\ \Delta\sigma_2=0$
Hollow cylinder	Compression-torsional	0.277	$\sigma_{a\theta}/\Delta\sigma_a=-1.003,\ \Delta\sigma_a<0,\ \Delta\sigma_r=\Delta\sigma_\theta=0$
	Extension-torsional	0.723	$\sigma_{a\theta}/\Delta\sigma_a=1.003,\ \Delta\sigma_a>0,\ \Delta\sigma_r=\Delta\sigma_\theta=0$

Determination of Material Parameters

The material constants ρ, γ and the initial value F_0 are determined so as to fit the test result of isotropic consolidation. The Poisson's ratio ν is obtained by the value of γ and the modulus of the initial rising part of the stress-strain curve in the triaxial compression test results, while almost elastic deformation proceeds in that part. The parameter u_R in the evolution rule of the normal-yield ratio R is determined from the curvature of the stress-strain curve in the transitional state from the elastic to the normal-yield state, while it is smaller for looser samples. The angle ϕ_c of internal friction in the critical state can be determined approximately from the stress ratio in the residual state. The limit-angle ϕ_b of the rotational hardening and the parameter b_r controlling the rate of rotational hardening are determined so as to supplement the degree of hardening in the test result with the deviatoric deformation. The initial value s_0 of the similarity-center and the parameter c_s are selected such that the hysteresis loop is depicted realistically, leading to the appropriate description of cyclic loading behavior. μ and ϕ_d describe the isotropic hardening/softening behavior induced by the plastic deviatoric deformation, while they are smaller for denser samples. a_T, b_T and c_T in the tangential inelastic modulus are determined such that the tangential effect is appropriate, while it becomes more influential as R and χ increase.

Values of material parameters are given independently for dense and loose sand in the present simulation. The incorporation of the superloading surface (Asaoka et al., 2000a, b) into the subloading surface model would enable us to describe the deformation behavior of dense and loose sand unifyingly by use of an identical set of material parameters. Hereafter, it is desirable to incorporate the superloading surface into the present model, i.e. the extended subloading surface model with tangential inelasticity.

Proportional Loading Behavior

The tangential stress rate effect is independent of the proportional loading behavior and thus the tangential strain rate $\mathbf{D}^t$ is not induced in this behavior. In the true triaxial test the b-value describing the state of intermediate principal stress is defined by;

$$b\equiv\frac{\sigma_2-\sigma_1}{\sigma_3-\sigma_1}, \tag{61}$$

where σ_1, σ_2 and σ_3 represent the minor, intermediate and major principal stresses, respectively, $b=0$ and 1 corresponding to the axisymmetric compression and extension states, respectively. For $\sigma_2=$const., the ratio of increments of the major and minor principal stresses is given by;

$$\frac{\Delta\sigma_3}{\Delta\sigma_1}=\frac{b-1}{b}, \tag{62}$$

where $\Delta(\ )$ stands for an increment.

In the hollow cylinder test when the radial stress σ_r and the peripheral stress σ_θ are constant during shear loading process, the major principal stress σ_3 and the minor principal stress σ_1 are given by the axial stress increment $\Delta\sigma_a$ and the torsional shear stress $\sigma_{a\theta}$ as follows:

$$\left.\begin{aligned}&\sigma_r=\sigma_\theta=\sigma_{m0},\\ &\left.\begin{matrix}\sigma_3\\ \sigma_1\end{matrix}\right\}=\sigma_{m0}+\frac{\Delta\sigma_a}{2}\mp\sqrt{\left(\frac{\Delta\sigma_a}{2}\right)^2+\sigma_{a\theta}^2},\\ &\sigma_a=\sigma_{m0}+\Delta\sigma_a,\end{aligned}\right\} \tag{63}$$

while the intermediate principal stress σ_2 corresponds to the radial stress σ_r. By substituting Eq. (63) into Eq. (61), the b-value for the hollow cylinder test is given as;

$$b=\frac{1}{2}\left\{1\pm\frac{1}{\sqrt{1+(2\sigma_{a\theta}/\Delta\sigma_a)^2}}\right\} \tag{64}$$

$$(+:\Delta\sigma_a>0,\ -:\Delta\sigma_a<0)$$

From Eq. (64), the ratio of the torsional stress to the axial stress increment is given as;

$$\frac{\sigma_{a\theta}}{\Delta\sigma_a}=\pm\frac{1}{2}\sqrt{\frac{1}{(2b-1)^2}-1} \tag{65}$$

$$(+:\Delta\sigma_a>0,\ -:\Delta\sigma_a<0)$$

Five types of tests for Reid Bedford sand are simulated by the extended subloading surface model, while the test conditions are summarized in Table 2 with the b-value and the relations of stress increment. The unique sets of the initial values of state variables and material constants are determined from the test data of the proportional loadings as listed in Table 3. The comparisons with the predicted and the measured results are shown in Figs. 6–10: The isotropic cyclic loading by the true triaxial test apparatus in Fig. 6, the axisymmetric compression with a constant lateral stress by the true triaxial test apparatus in Fig. 7, the proportional loading with $b=0.277$ by the true triaxial test apparatus in Fig. 8 and the proportional loading with $b=0.277$ by the hollow cylinder test appara-

Table 3. The initial values and material constants for Reid Bedford sand

Material constants	Frictional angle in the axisymmetric compression			ϕ_c (degree)	27
	Hardening/softening	Isotropic	Volumetric	ρ	0.0045
			Deviatoric	μ	0.8
				ϕ_d (degree)	27.5
		Rotational		b_r	70
				ϕ_b (degree)	20
	Evolution of R			u_R	50
	Movement of similarity-center			c_s	15
	Elastic constant			γ	0.0025
	Poisson's ratio			ν	0.3
Initial values of material parameters				F_0 (kPa)	180
				β_0	0
				s_0 (kPa)	0
				σ_0 (kPa)	$-100\mathbf{I}$

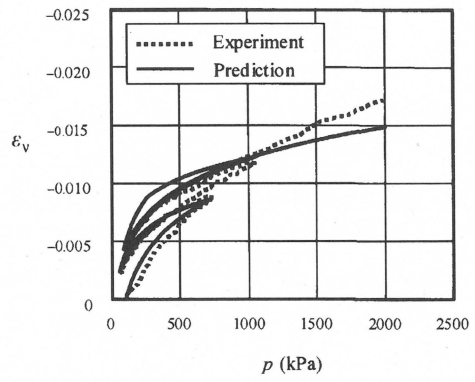

Fig. 6. Simulation result of the cyclic isotropic loading by the true triaxial test apparatus (Reid Bedford sand)

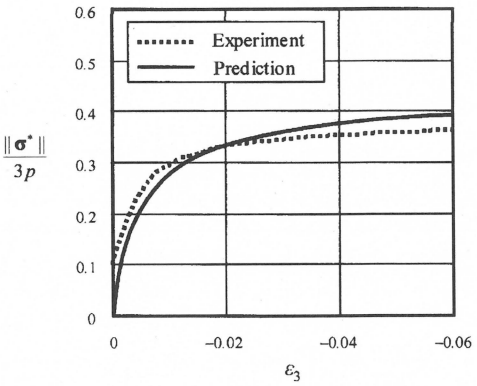

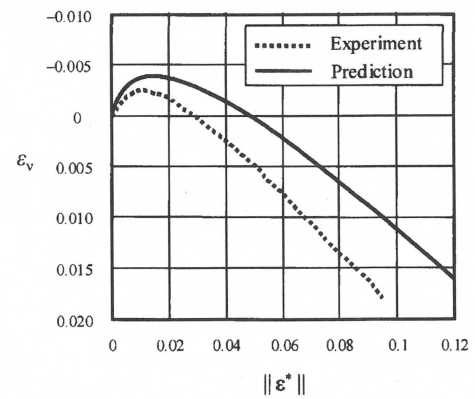

Fig. 7. Simulation results of the axisymmetric compression with a constant lateral stress by the true triaxial test apparatus (Reid Bedford sand)

tus in Fig. 9 and the proportional loading with $b=0.723$ by the hollow cylinder test apparatus in Fig. 10, where ε_v is the volumetric strain. The sufficiently good simulations are observed except for a part of them, e.g. ε_v in Fig. 7, ε_1, ε_2, ε_3 in Fig. 8, $\sigma_{a\theta}$ in Fig. 10, while same values for all the material parameters are used in the calculations.

In all the analyses, the model simulates well the experiments using the unique set of material parameters in spite of the wide variety of test types. Further, the hysteresis loops in the cyclic isotropic loading are properly described by the translation of similarity-center. Beside, Figs. 11 and 12 show the simulation results of the axisymmetrical cyclic loading under the undrained and drained conditions for Toyoura sand, which is widely used in Japan for the study of the strength and deformation characteristics of sands. The material parameters for Toyoura sand are listed in Table 4. The predictions represent well the stress and strain paths of the experiments. Thus, it can be stated that the extended subloading surface model has the high capability of predicting the proportional loading behavior including cyclic loading process.

Nonproportional Loading Behavior

The loading of circular stress path in π-plane in which stress rate has a significant component tangential to the

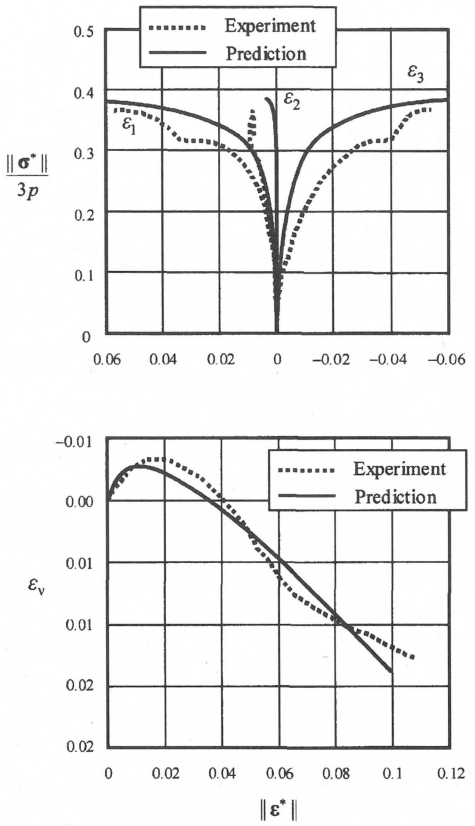

Fig. 8. Simulation results of the proportional loading with $b=0.277$ by the true triaxial test apparatus (Reid Bedford sand)

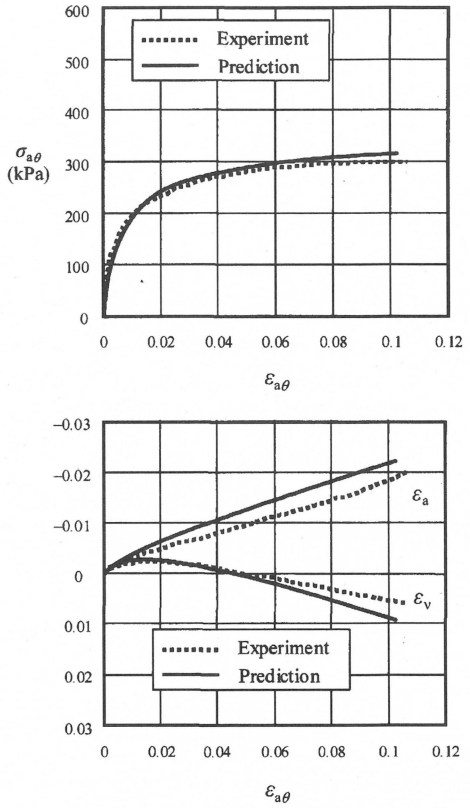

Fig. 9. Simulation results of the proportional loading with $b=0.277$ by the hollow cylinder test apparatus (Reid Bedford sand)

subloading surface is the typical nonproportional loading. The test was performed by the true triaxial apparatus, where the principal stresses are varied individually leading to the circular stress path in deviatoric stress plane, keeping the magnitude of the deviatoric stress $\|\sigma^*\|$ and the mean principal stress σ_m constant as shown in Fig. 13. The loading process for Reid Bedford sand is as follows:

(i) The proportional deviatoric loading process: σ_3 is decreased to -559 kPa from the isotropic stress state of $\sigma_{m0}=-345$ IkPa, while σ_1 and σ_2 are both proportionately increased to -238 kPa, keeping the mean principal stress σ_m at -345 kPa. The magnitude of the deviatoric stress $\|\sigma^*\|$ finally becomes 262 kPa.

(ii) The loading process of the circular stress path: The principal stresses are varied sinusoidally, keeping the magnitude of deviatoric stress $\|\sigma^*\|$ and the mean principal stress σ_m constant, while the principal stresses are described as

$$\left.\begin{aligned}\sigma_1&=\sigma_m+\sqrt{\frac{2}{3}}\|\sigma^*\|\cos\theta_\sigma,\\ \sigma_2&=\sigma_m+\sqrt{\frac{2}{3}}\|\sigma^*\|\cos\left(\theta_\sigma-\frac{2}{3}\pi\right),\\ \sigma_3&=\sigma_m+\sqrt{\frac{2}{3}}\|\sigma^*\|\cos\left(\theta_\sigma+\frac{2}{3}\pi\right).\end{aligned}\right\} \tag{66}$$

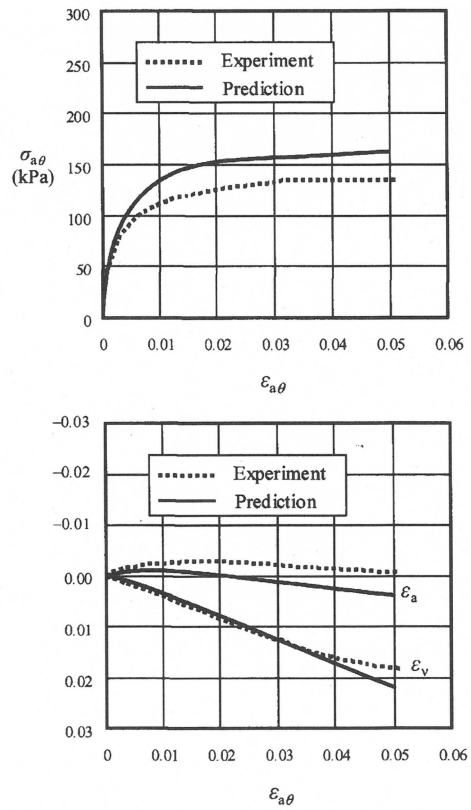

Fig. 10. Simulation results of the proportional loading with $b=0.723$ by the hollow cylinder test apparatus (Reid Bedford sand)

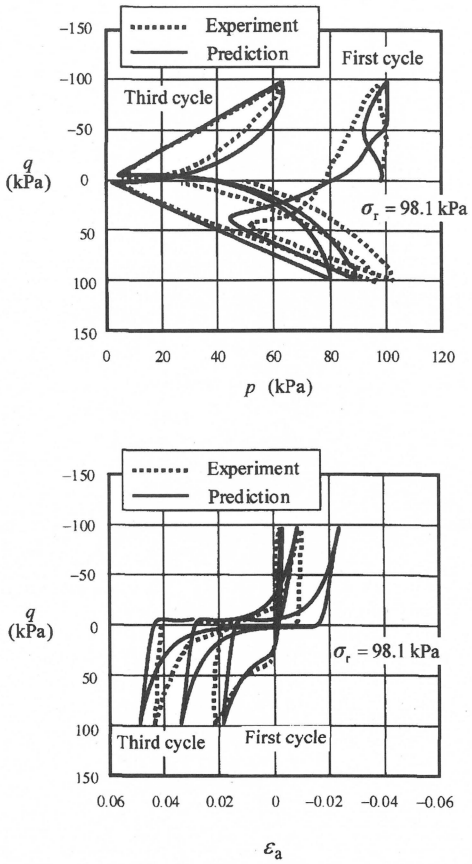

Fig. 11. The cyclic triaxial test with the constant stress amplitude $q = \pm 98$ kPa under the undrained condition for the dense specimen of Toyoura sand (Tatsuoka et al., 1986)

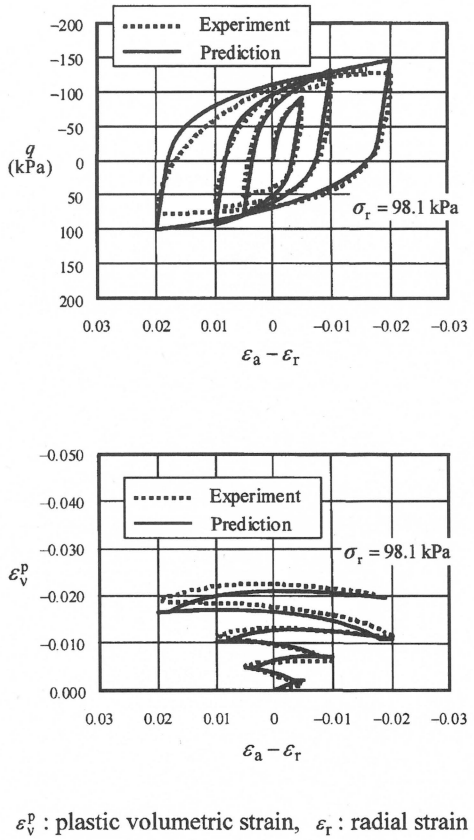

Fig. 12. The cyclic triaxial test performed at a constant $p(=98.1$ kPa) under drained condition for the loose specimen of Toyoura sand (Pradhan et al., 1989)

Table 4. The initial values and material constants for specimens of Toyoura sand

State of specimen					Dense	Loose
Material constants	Frictional angle in the axisymmetric compression			ϕ_c (degree)	32	32
	Hardening/softening	Isotropic	Volumetric	ρ	0.0018	0.0045
			Deviatoric	μ	0.8	1
				ϕ_d (degree)	29	30
		Rotational		b_r	100	80
				ϕ_b (degree)	20	17
	Evolution of R			u_R	15	10
	Movement of similarity-center			c_s	100	1
	Elastic constant			γ	0.001	0.0017
	Poisson's ratio			ν	0.3	0.3
Initial values of material parameters				F_0 (kPa)	350	50
				β_0	0	0
				s_0 (kPa)	0	0
				σ_0 (kPa)	$-29.4\mathbf{I}$	$-29.4\mathbf{I}$

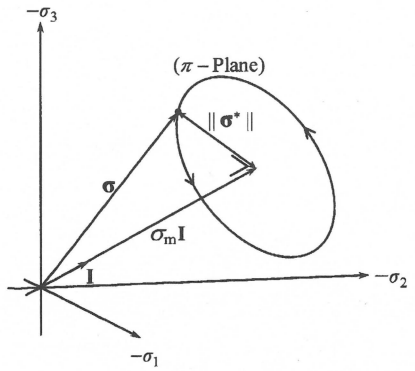

Fig. 13. Circular stress path in π-plane

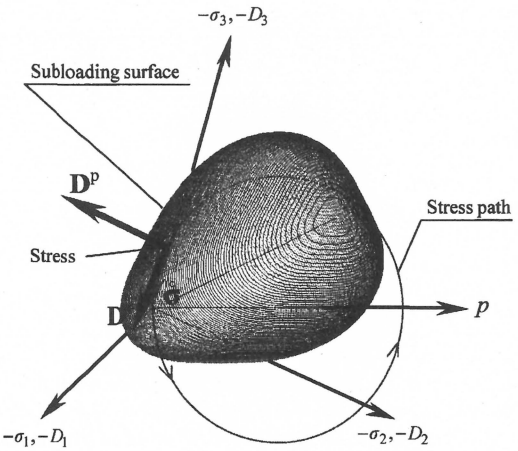

Fig. 14. The subloading surface in stress space during the loading process of circular stress path

Table 5. The material constants in the tangential inelastic modulus for Reid Bedford sand

Tangential inelastic modulus T	a_T	0.008
	b_T	3
	c_T	1

Then, the increments of the principal stresses for the circular stress path are given by

$$\left.\begin{aligned}\Delta\sigma_1 &= -\sqrt{\frac{2}{3}}\|\boldsymbol{\sigma}^*\|\sin\theta_\sigma\Delta\theta_\sigma,\\ \Delta\sigma_2 &= -\sqrt{\frac{2}{3}}\|\boldsymbol{\sigma}^*\|\sin\left(\theta_\sigma-\frac{2}{3}\pi\right)\Delta\theta_\sigma,\\ \Delta\sigma_3 &= -\sqrt{\frac{2}{3}}\|\boldsymbol{\sigma}^*\|\sin\left(\theta_\sigma+\frac{2}{3}\pi\right)\Delta\theta_\sigma.\end{aligned}\right\} \quad (67)$$

The Lode angle θ_σ is varied from 60° to 780° realizing the two cycles.

The material parameters in Table 3 determined from the proportional loading behavior are used as they are in the analysis because of the identical initial state of the specimen, and the material constants in the tangential inelastic modulus T are selected as listed in Table 5.

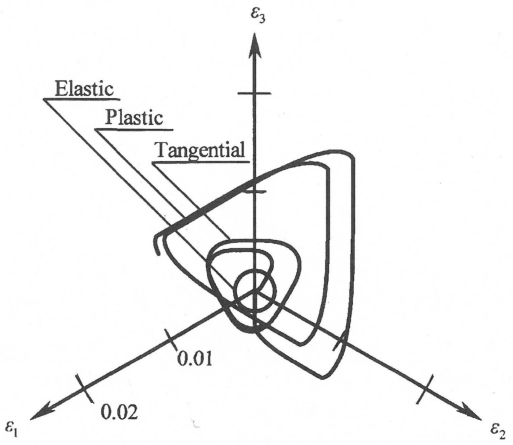

Fig. 15. Predicted the elastic, plastic and tangential strain paths in π-plane (Reid Bedford sand)

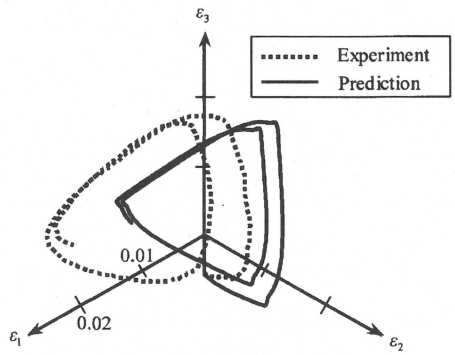

(a) without the tangential strain rate

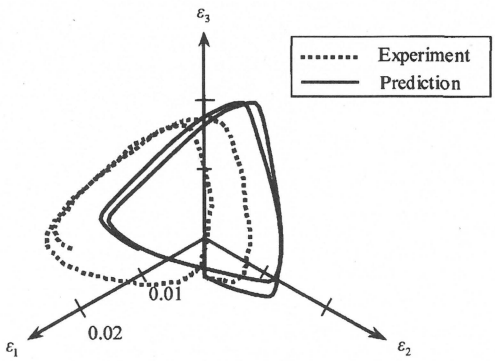

(b) with the tangential strain rate

Fig. 16. Strain paths in π-plane (Reid Bedford sand)

The state of the subloading surface in principal stress space during the loading process of circular stress path in π-plane is depicted in Fig. 14, and the stress rate $\mathring{\boldsymbol{\sigma}}$, plastic strain rate $\mathbf{D}^p$ and the tangential strain rate $\mathbf{D}^t$ are also shown in the figure. The calculated plastic strain and tangential strain paths in π-plane are depicted in Fig. 15. The plastic strain path exhibits the similar shape to the

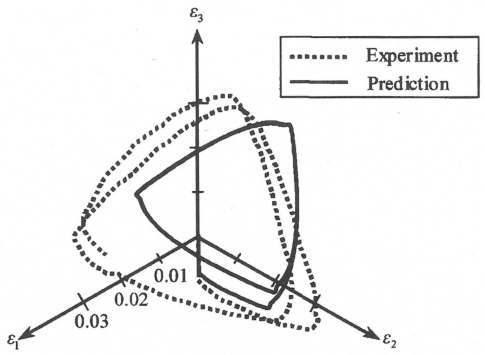

(a) without the tangential strain rate

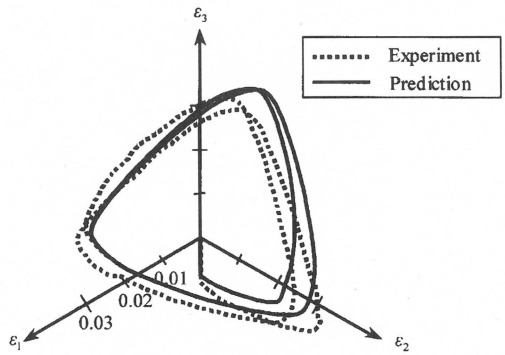

(b) with the tangential strain rate

Fig. 17. Strain paths in π-plane (Hostun sand)

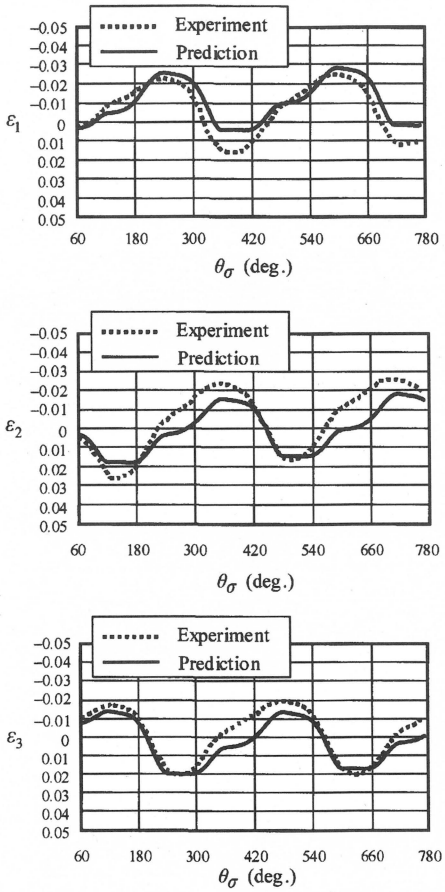

Fig. 18. Variations of three principal strains ε_1, ε_2, ε_3 predicted by the extended subloading surface model without the tangential strain rate vs. θ_σ (Hostun sand)

Table 6. The initial values and material constants for Hostun sand

Material constants	Frictional angle in the axisymmetric compression			ϕ_c (degree)	30
	Hardening/softening	Isotropic	Volumetric	ρ	0.008
			Deviatoric	μ	1
				ϕ_d (degree)	31
		Rotational		b_r	40
				ϕ_b (degree)	24
	Evolution of R			u_R	60
	Movement of similarity-center			c_s	50
	Elastic constant			γ	0.0035
	Poisson's ratio			ν	0.3
	Tangential inelastic modulus T			a_T	0.018
				b_T	5
				c_T	1
Initial values of material parameters				F_0 (kPa)	600
				β_0	0
				s_0 (kPa)	$-20\mathbf{I}$
				σ_0 (kPa)	$-100\mathbf{I}$

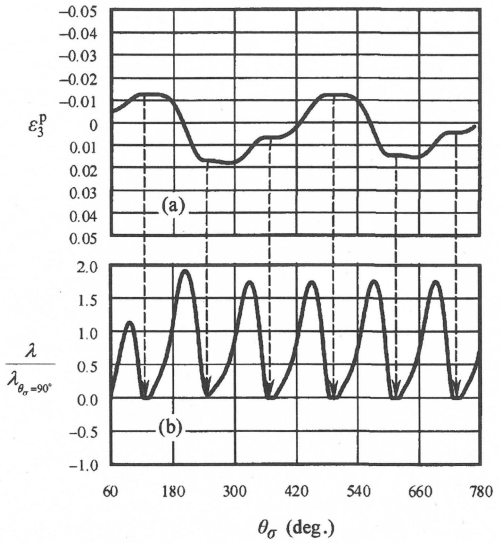

Fig. 19. The variations of the plastic strain component in ε_3 and the value of $\lambda/\lambda_{\theta\sigma}=90°$ vs. θ_σ (Hostun sand)

π-section of the subloading surface with the rotation of $\pi/2$ in the clockwise direction because the plastic strain rate occurs perpendicular to the subloading surface according to the associated flow rule. On the other hand, the tangential strain rate is tangential to the subloading surface, and then the tangential strain path exhibits the similar shape to the subloading surface in π-plane. It gradually develops depending on the normal-yield ratio R, fulfilling both the continuity and the smoothness conditions. The elastic strain path is also depicted in the figure. The elastic strain component is small compared with the inelastic strains, while the direction of the elastic strain rate is parallel to the stress rate.

The strain path in π-plane predicted by the model without the tangential strain rate is indicated in Fig. 16(a) comparing with the test data. The shapes of both strain paths in the test data and the prediction are similar to each other. The predicted strain path is small compared with the measured path and inclines in the clockwise direction from the latter. The size and the direction of the strain path are improved by the incorporation of the tangential strain rate as shown in Fig. 16(b). Besides, the measured and the predicted strain paths without and with the tangential strain rate for Hostun sand are shown in Figs. 17(a) and (b), while the magnitude of the deviatoric stress $\|\boldsymbol{\sigma}^*\|$ is 420 kPa. The selected material parameters are listed in Table 6. It is clearly exhibited that the prediction is improved by the incorporation of tangential stress rate effect.

The variations of the principal strains ε_1, ε_2, ε_3 against the Lode angle θ_σ for Hostun sand by the model without the tangential strain rate are indicated in Fig. 18 comparing with the test data. The variation in the plastic principal strain component ε_3^p vs. the Lode angle θ_σ is depicted in Fig. 19(a) and the variations of the values of $\lambda/\lambda_{\theta\sigma=90°}$, $\lambda_{\theta\sigma=90°}$ represents the value of λ at $\theta_\sigma=90°$, is indicated in Fig. 19(b). It is observed that the states of

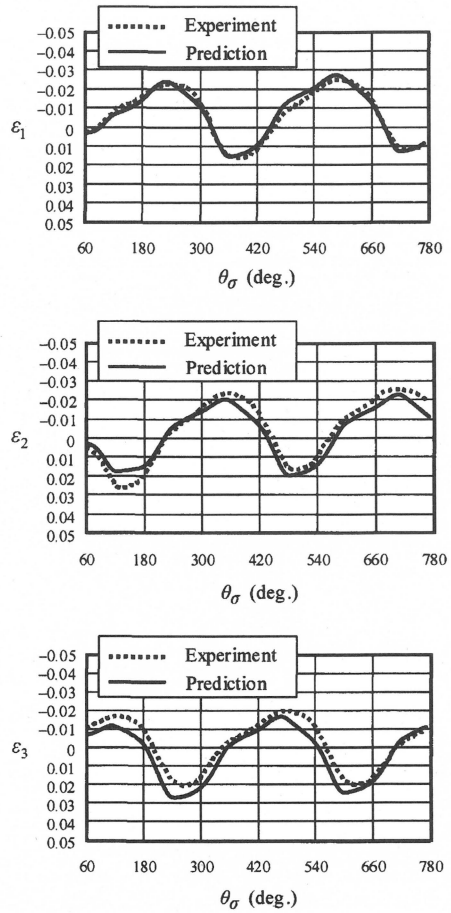

Fig. 20. Variations of three principal strains ε_1, ε_2, ε_3 predicted by the extended tangential-subloading surface model vs. θ_σ (Hostun sand)

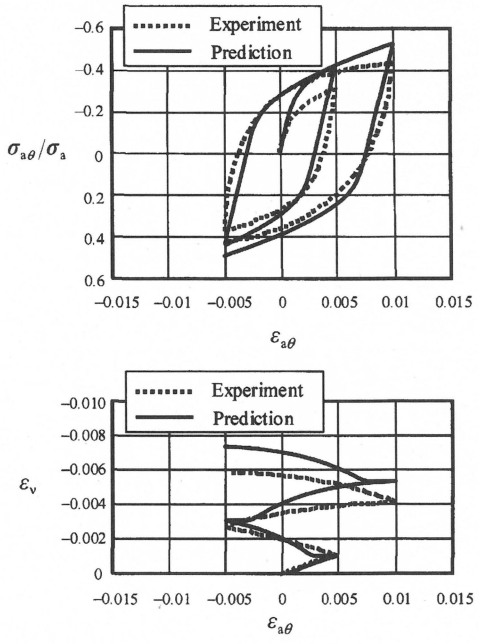

Fig. 21. Simulation results by the extended subloading surface model without the tangential strain rate for the torsional simple shear test performed at a constant $\sigma_a=-98.1$ kPa under drained condition for the loose specimen of Toyoura sand (Pradhan et al., 1989)

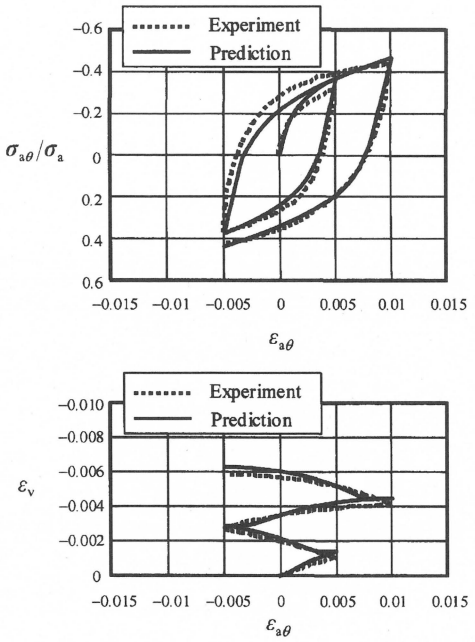

Fig. 22. Simulation results by the extended tangential-subloading surface model for the torsional simple shear test performed at a constant $\sigma_a = -98.1$ kPa under drained condition for the loose specimen of Toyoura sand (Pradhan et al., 1989)

Table 7. The material constants in the tangential inelastic modulus T for the loose specimen of Toyoura sand

a_T	0.08
b_T	3
c_T	1

deformation without inelastic strain rate appear periodically. It would be the reason why the predicted results differ from test data. On the other hand, principal strains ε_1, ε_2, ε_3 are predicted well by the model with the tangential strain rate as shown in Fig. 20.

Figures 21 and 22 show the simulation results without and with the tangential strain rate for the torsional simple shear test under the drained condition for the loose specimen of Toyoura sand, where the axial stress σ_a is constant at -98.1 kPa and the peripheral and radial strains ε_θ, ε_r are kept at zero during the shear loading process. The material parameters of the loose state in Tables 4 and 7 are used as they are in the calculations. The shear stress and volumetric strain paths are improved incorporating the tangential stress rate effect.

Eventually, it could be concluded that the tangential strain rate has to be incorporated into the elastoplastic constitutive model for describing the nonproportional loading behavior of soils.

CONCLUDING REMARKS

The validity of the extended tangential-subloading surface model for the prediction of deformation behavior of soils was studied by comparing with the test data of various sands, i.e. Reid Bedford and Toyoura sands with Hostun sand. Then, it is verified that this model is capable of describing general deformation behavior of sands subjected to various loadings ranging from the proportional to the cyclic-nonproportional loading processes. Eventually, it can be concluded that the mechanical properties 1)-6) described in the introduction have to be incorporated for the constitutive equation of sands exhibiting complex deformation behavior compared with metals and clays. Especially, it is revealed that the incorporation of the tangential stress rate effect is of importance for the description of nonproportional loading behavior, which has not been considered in the previous formulation (cf. Hashiguchi and Chen, 1998).

It is required to determine material parameters appropriately and easily for the application of constitutive models. If not, they will not be utilized actually. To this aim, measurements of material parameters and applications to the description of deformation behavior of materials should be accumulated so as to provide the database. The wide capability of the extended tangential-subloading surface model to the description of deformation behavior of soils is verified by comparing newly with various proportional and cyclic-nonproportional loading test data of Reid Bedford and Toyoura sands with Hostun sand in this article.

REFERENCES

1) Armstrong, P. J. and Fredericson, C. O. (1966): A mathematical representation of the multiaxial Bauschinger effect, *G. E. G. B Report RD/B/N*, p. 731.
2) Asaoka, A., Nakano, M. and Noda, T. (2000a): Superloading yield surface concept for highly structured soil behaviour, *Soils and Foundations*, **40**(2), 99–110.
3) Asaoka, A., Nakano, M., Noda, T. and Kaneda, K. (2000b): Delayed compression/consolidation of natural clay due to degradation of soil structure, *Soils and Foundations*, **40**(3), 75–85.
4) Dafalias, Y. F. (1985): The plastic spin, *J. Appl. Mech.*, ASME, **52**, 865–871.
5) Dafalias, Y. F. and Popov, E. P. (1975): A model of nonlinearly hardening materials for complex loading, *Acta Mech.*, **21**, 173–192.
6) Drucker, D. C. (1988): Conventional and unconventional plastic response and representation, *Appl. Mech. Rev.*, ASME, **41**, 151–167.
7) Hashiguchi, K. (1974): Isotropic hardening theory of granular media, *Proc. JSCE*, **227**, 45–60.
8) Hashiguchi, K. (1978): Plastic constitutive equations of granular materials, *Proc. US-Japan Seminar Continuum Mech. Stast. Appr. Granular Materials*, Sendai, 321–329.
9) Hashiguchi, K. (1980): Constitutive equations of elastoplastic materials with elastic-plastic transition, *J. Appl. Mech.*, ASME, **47**, 266–272.
10) Hashiguchi, K. (1989): Subloading surface model in unconventional plasticity, *Int. J. Solids Strut.*, **25**, 917–945.
11) Hashiguchi, K. (1993a): Fundamental requirements and formulation of elastoplastic constitutive equations with tangential plasticity, *Int. J. Plasticity*, **9**, 525–549.
12) Hashiguchi, K. (1993b): Mechanical requirements and structures of cyclic plasticity models, *Int. J. Plasticity*, **9**, 721–748.
13) Hashiguchi, K. (1995): On the linear relation of V-ln$p$ and ln v-ln p for isotropic consolidation of soils, *Int. J. Numer. Anal. Meth. Geomech.*, **19**, 367–376.
14) Hashiguchi, K. (1997): The extended flow rule in plasticity, *Int. J.*

Plasticity, **13**, 37–58.
15) Hashiguchi, K. (1998): The tangential plasticity, *Metals and Materials*, **4**, 652–656.
16) Hashiguchi, K. (2000): Fundamentals in constitutive equation: continuity and smoothness conditions and loading criterion, *Soils and Foundations*, **40**(4), 155–161.
17) Hashiguchi, K. (2001): Description of inherent/induced anisotropy of soils: Rotational hardening rule with objectivity, *Soils and Foundations*, **41**(6), 139–145.
18) Hashiguchi, K. (2002): A proposal of the simplest convex-conical surface for soils, *Soils and Foundations*, **42**(3), 107–113.
19) Hashiguchi, K. (2005): Generalized plastic flow rule, *Int. J. Plasticity*, **21**, 321–351.
20) Hashiguchi, K. and Chen, Z.-P. (1998): Elastoplastic constitutive equations of soils with the subloading surface and the rotational hardening, *Int. J. Numer. Anal. Meth. Geomech.*, **22**, 197–227.
21) Hashiguchi, K. and Tsutsumi, S. (2001): Elastoplastic constitutive equation with tangential stress rate effect, *Int. J. Plasticity*, **17**, 117–145.
22) Hashiguchi, K. and Ueno, M. (1977): Elastoplastic constitutive laws of granular materials, *Constitutive Equations of Soils, Proc. 9th ICSMFE Spec. Session 9, Tokyo, JSSMFE, 73–82.*
23) Hill, R. (1950): *The Mathematical Theory of Plasticity*, Clarendon Press.
24) Iizuka, A., Tachibana, S., Kawai, K. and Ohta, H. (2005): Changes in instantaneous shear modulus of normally consolidated clay with shear history, *Soils and Foundations*, **45**(2), 135–144.
25) Iwan, W. D. (1967): On a class of models for the yielding behavior of continuous and composite systems, *J. Appl. Mech.*, ASME, **34**, 612–617.
26) Krieg, R. D. (1975): A practical two surface plasticity theory, *J. Appl. Mech.*, ASME, **42**, 641–646.
27) Lemaitre, J. and Chaboche, J. L. (1990): *Mechanics of Solid Materials*, Cambridge Univ. Press.
28) Masing, G. (1926): Eigensppannungen und verfestigung beim messing, *Proc. 2nd Int. Congr. Appl., Mech.*, Zurich, 332–335.
29) Mroz, Z. (1966): On forms of constitutive laws for elastic-plastic solids, *Archiwum Mechaniki Stosowanej*, **18**, 1–34.
30) Mroz, Z. (1967): On the description of anisotropic work hardening, *J. Mech. Phys. Solids*, **15**, 163–175.
31) Nova, R. (1977): On the hardening of soils, *Arch. Mech. Stos.*, **29**, 445–458.
32) Pradhan, T. B. S., Tatsuoka, F. and Sato, Y. (1989): Experimental stress-dilatancy relations of sand subjected to cyclic loading, *Soils and Foundations*, **29**(1), 45–64.
33) Rudnicki, J. W. and Rice, J. R. (1975): Conditions for localization of deformation in pressure-sensitive dilatant materials, *J. Mech. Phys. Solids*, **23**, 371–394.
34) Saada, A. S. and Bianchini, G. (1989): *Proc. Int. Workshop on Constitutive Equations for Granular Non-cohesive Soils*, Cleveland, Balkema, Rotterdam.
35) Sekiguchi, H. and Ohta, K. (1977): Induced anisotropy and time dependency in clays, *Constitutive Equations of Soils (Proc. 9th ICSMFE, Spec. Session* 9, Tokyo), JSSMFE, 229–238.
36) Tatsuoka, F., Toki, S., Miura, S., Kato, H., Okamoto, M., Yamada, S., Yasuda, S. and Tanizawa, F. (1986): Some factors affecting cyclic undrained triaxial strength of sand, *Soils and Foundations*, **26**(3), 99–116.
37) Wilde, P. (1977): Two invariants depending models of granular media, *Arch. Mech. Stos.*, **29**, 799–809.
38) Yatomi, C., Yashima, A., Iizuka, A. and Sano, I. (1989): General theory of shear bands formulation by a non-coaxial Cam-clay model, *Soils and Foundations*, **29**, 41–53.
39) Zbib, H. M. and Aifantis, E. C. (1988): On the concept of relative and plastic and its implications to large deformation theories, Part I: Hypoelasticity and vertex-type plasticity, *Acta Mech.*, **75**, 15–33.